J Mater Sci (2007) 42:2347–2357
DOI 10.1007/s10853-007-1593-y

Microstructural evolution of gold–aluminum wire-bonds

Adi Karpel · Giyora Gur · Ziv Atzmon · Wayne D. Kaplan

Received: 20 January 2007 / Accepted: 7 February 2007 / Published online: 12 March 2007
© Springer Science+Business Media, LLC 2007

Abstract The purpose of this study is to understand the morphological changes that occur during *annealing* of Al–Au wire-bonds, by analyzing the interface region of annealed model wire-bonded samples between 5N (99.999%) Au wires and Al pads. Due to the small length scale of the intermetallic region at the interface of the bond, the analysis was done using scanning/transmission electron microscopy combined with energy dispersive spectroscopy. Samples were prepared using a dual-beam focused ion beam system. Microstructural characterization showed that during annealing, a Au-rich intermetallic region was formed under the bond and at the periphery of the bond. Two types of failures occurred during annealing: crack formation at the bond periphery due to an increase in volume during intermetallic growth and the formation of stresses; and oxidation of the $AlAu_4$ phase adjacent to the Au ball, which resulted in the formation of continuous cracks between the Au ball and the intermetallic region. The characteristic void-line found inside the intermetallic region played no part in failure that occurred during exposure to elevated temperatures.

A. Karpel · W. D. Kaplan (✉)
Department of Materials Engineering, Technion – Israel Institute of Technology, Haifa 32000, Israel
e-mail: kaplan@tx.technion.ac.il

G. Gur · Z. Atzmon
Kulicke & Soffa Bonding Tools, Yokneam Elite 20692, Israel

Introduction

Wire ball-bonding is one of the key industrial techniques to connect a semiconductor chip to a mountable package. The connection to the chip is usually made between high purity (99.99%) Au wire and Al pads by the application of temperature and ultrasonic vibrations, which results in the formation of an Al–Au intermetallic region at the bond interface [1].

Exposure to elevated working temperatures can result in degradation of the electrical conductivity due to growth of the intermetallic region, and even a connection-failure due to the formation of cracks inside the bond [1–5]. Since one of the main assumptions regarding intermetallic formation during the wire-ball bonding process is that it occurs in the solid state, analysis of annealed thin Al–Au films is often used to simulate the phase transformations that occur in the Al–Au wire-bonding system during the device life cycle [6–10]. This analysis showed that during annealing of thin Al–Au films, a sequence of thermodynamically stable intermetallics are formed and continued to grow during annealing.

A characteristic phenomenon in the annealed intermetallic region of *real* Al–Au bonded systems is the presence of a void-line. Under the assumption that the intermetallic region forms in the solid-state, thin-film analysis led to the conclusion that void formation occurs due to the Kirkendall effect [2, 9, 11, 12], or due to volume changes that occur during Al–Au intermetallic formation and growth, which result in the formation of flaws in the intermetallic region [2, 3].

To date, most of the microstructural characterization of wire bonds has been done using scanning electron microscopy (SEM) combined with energy

dispersive spectroscopy (EDS). SEM–EDS analysis of samples annealed for different durations and at different annealing temperatures showed that Al–Au intermetallics, which are formed during the bonding stage, continue to grow by diffusion during annealing. Morphological changes in the Al–Au intermetallic region were the main indication for the change in composition of the intermetallics [1–9]. The length-scale of most of the intermetallic regions in Al–Au wire-bonds is sub-micron. At the same time, the lateral resolution of SEM–EDS depends on the electron–photon interaction volume, which, for the Al–Au system, can reach a few microns [13, 14]. As such, the lateral resolution of SEM–EDS is insufficient for analysis of the intermetallic regions in Al–Au wire-bonds. Therefore, the present work is based on analysis of thin samples by scanning/transmission electron microscopy (S/TEM) combined with EDS.

Conventional TEM specimen preparation techniques cannot be applied to wire bonds due to the requirement for site-specific analysis inside the bond region. Therefore, in this study, TEM sample preparation was conducted using a dual-beam focused ion beam (FIB) system [15], which can provide both site-specific analysis of a region in the bond and statistical analysis of the different failure morphologies that occur during extended exposure to elevated temperatures.

Our previous work on *as-bonded* Al–Au wire-bonds showed that a liquid state could form during wire bonding [16]. Therefore, microstructural analysis of the intermetallic region of annealed wire bonds has to be conducted on *real* Al–Au wire-bonds, rather than annealed Al–Au thin films. In this work, FIB and TEM were applied to understand the morphological evolution of Al–Au wire-bonds as a function of thermal annealing.

Experimental methods

Materials and processing

Uniform Al-1.0 wt.% Si pads (1 μm in thickness) were deposited on thermally oxidized Si wafers. The Si wafers were diced, and die-attached prior to wire bonding. A 17.8 μm diameter model Au wire of 99.999% purity (5N) was used for wire bonding. Wire bonding was performed on a K&S model 8028 PPS automatic wire bonder. The ball bond diameter was kept within 31 ± 2 μm. Thermosonic ball bonding of each Si die was performed at 165 °C for an average time of less than ~30 s for each set of bonds on a die, with a maximum pre-heat and post-heat time of ~45 s at 150 °C. The bonding parameters were optimized and the resultant average bond shear force was 7.2 gr [1].

In addition to as-bonded samples, wire-bonds were annealed for 30 min, 2, 24, 48, 72 and 100 h at 175 °C in air without encapsulation. Thermal treatments were used to simulate an accelerated thermal exposure characteristic of device operation conditions.

Characterization

The TEM and SEM samples were prepared using a FEI Strata 400s dual-beam FIB. SEM specimens were prepared from the wire bonds by rough preliminary cross-sectioning at an accelerating voltage of 30 kV and a Ga+ ion beam current of 21 nA, followed by fine polishing at an ion current of 93 pA. Subsequent ion beam exposures at 93 pA were used to expose the morphology of the intermetallic phases in the polished cross-sections.

The morphology of the Au ball-bond was analyzed prior to and after the wire bonding process from secondary electron (SE) micrographs generated from scanning ion microscopy (SIM) at a Ga+ ion current of 93 pA. The contrast in SIM is influenced by the ion channeling effect, where the amount of secondary electrons that escape from the surface of the sample is a function of the depth of penetration of the ion beam inside the lattice. The depth of penetration depends on the orientation of the crystal lattice, as presented schematically in Fig. 1 [15].

Specimens for S/TEM were prepared from the wire bond samples using the lift-out technique [15]. Rough preliminary cross-sections were made at a Ga+ ion current of 21 nA (30 kV), and fine polishing was done at 93 pA. During the sample preparation for TEM, Ga^+ ion bombardment can result in the formation of a high density of dislocation loops inside the Au grains [17].

TEM analysis was done at 200 kV using a JEOL 2000FX equipped with EDS (Thermo Noran) and a Tecnai F20 G^2 FEG-TEM, equipped with a high angle annular dark field (HAADF) STEM detector and EDS (EDAX). EDS in the FEG-TEM was conducted using a beam diameter of ~1 nm.

EDS analysis was done in STEM mode by scanning a specific area inside a grain. In this way, the average composition of each grain could be determined. For regions with an extremely fine microstructure, EDS point analysis was conducted using a ~1 nm diameter electron beam. In order to improve the statistics from point analysis, numerous points were analyzed in each region. EDS quantification was made using the Cliff–

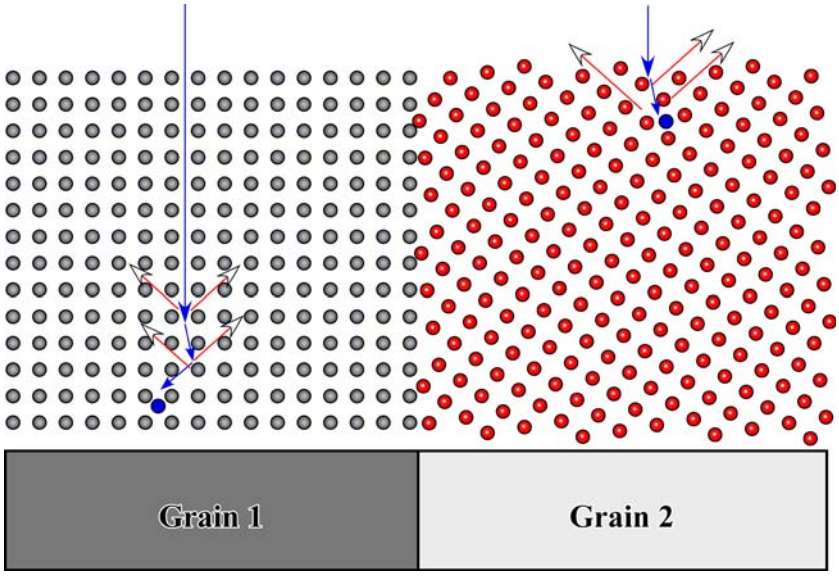

Fig. 1 A schematic drawing of the change in contrast due to the orientation of the lattice during SIM. Grain 1 is oriented close to a low-index zone axis, so the incident ions channel into the crystal before significant inelastic scattering. As a result the distance to the surface is greater than the mean-free-path of secondary electrons, and the grain will appear with a dark contrast. Grain 2 is not oriented in a low-index zone axis, so secondary electrons produced by inelastic scattering of the incident ions can escape from the surface and reach the detector, resulting in a light contrast from this grain

Lorimar approximation with calculated standards for calibration. Due to the lack of reference samples, the error in this analysis can reach ~20%.

Results

Analysis of the morphology prior to annealing

The free air ball (FAB)

The first stage of the wire bonding process is the formation of the Au FAB. This is described in Fig. 2 by a schematic drawing and a SE SIM micrograph. During this process, the wire tip is melted by an electrical spark, and a round shape results from the surface energy of the liquid Au. Solidification of the FAB results in the formation of large grains in the FAB and grain growth in the heat affected zone (HAZ) of the adjacent wire, due to heat transfer during the solidification process [1]. TEM analysis of the FAB region (Fig. 3) shows the presence of large grains and a relatively low dislocation density, due to the solidification process. In addition to bend-contours in the bright field (BF) diffraction contrast micrograph in Fig. 3, radiation damage in the form of dislocation loops is easily detected in the Au grains. The radiation damage is due to the ion milling process used to prepare the TEM specimens [17].

The as-bonded state

The bond region that is formed during the wire bonding process is presented in the SE SIM micrograph in Fig. 4. The bond is based on the formation of an intermetallic region at the Al–Au interface. As shown in Fig. 4, an intermetallic region was not formed in the periphery region of the bond. This can be attributed to the fact that the periphery region is formed by plastic deformation that squeezes the ball out of the capillary during the wire bonding process. Therefore, this region is subjected only to ultrasonic vibration without the main component of the vertical force that forms the bond under the center of the capillary. This can result in the formation of a gap between the Al pad and the Au ball along the periphery [11].

The wire-bonding process results in plastic deformation of the Au ball. The relatively large Au grains in the Au ball and a smaller grain size in the area adjacent to the intermetallic region are visible in Fig. 4. In order to understand the morphological changes that occur during the wire bonding process, the morphology of the Au ball-bond was analyzed by TEM. Figure 5 presents a BF TEM micrograph of the Au ball in the as-bonded state. The sample was prepared from the center of the bond region (see inset in Fig. 5). A relatively high density of dislocations are visible in the Au adjacent to the Al–Au interface, with sub-grains

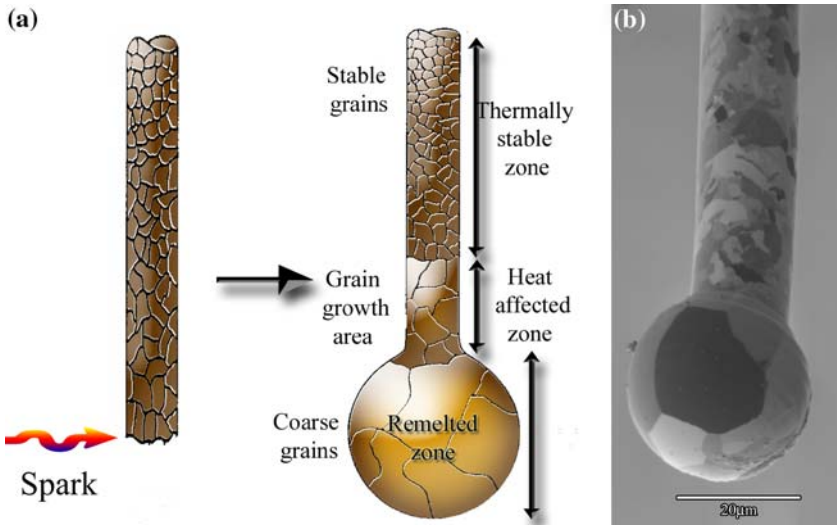

Fig. 2 (**a**) Schematic drawing of the morphology changes that occur during FAB formation; (**b**) Secondary electron micrograph of a FAB at the tip of a wire, presenting the morphological changes that occur during FAB formation

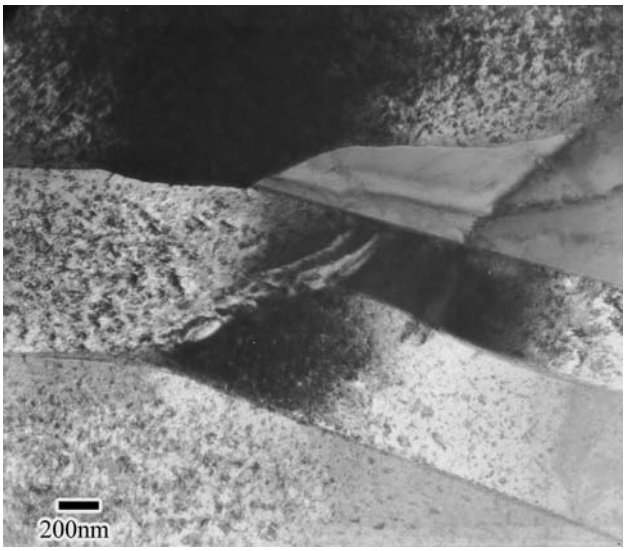

Fig. 3 BF TEM micrograph of a 5N FAB presenting anisotropic grains and a relatively low dislocation density

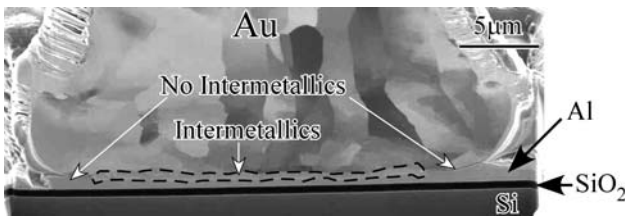

Fig. 4 SE SIM micrograph of a cross-section of an as-bonded sample presenting the formation of an intermetallic region, and the absence of an intermetallic region at the periphery of the bond

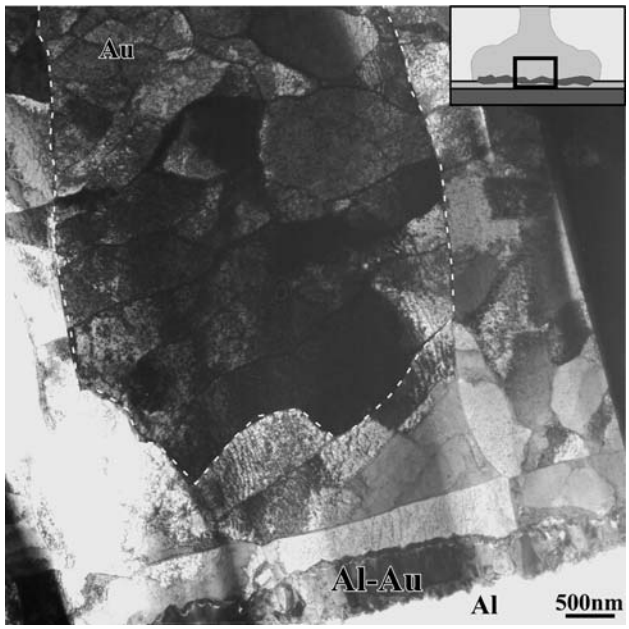

Fig. 5 BF TEM micrograph of the region indicated by the schematic drawing, presenting the Al–Au reaction region between the Al pad and the Au ball, and also the grain morphology of the gold ball. The dashed-line indicates a Au grain containing low angle grain boundaries

forming inside the Au ball. A comparison between the morphology of the FAB (Fig. 3) and the morphology of the Au after the bonding process indicates that the relatively high density of the dislocations is a result of plastic deformation during the bonding process.

The formation of sub-grains inside the large Au grains indicates that a recovery process occurs during the bonding process, by dislocation movement to form low angle grain boundaries (LAGB), which cannot be detected in the SE SIM mode.

A higher magnification BF TEM micrograph of the bond region in the as-bonded state is presented in Fig. 6. A void-line inside the intermetallic region that

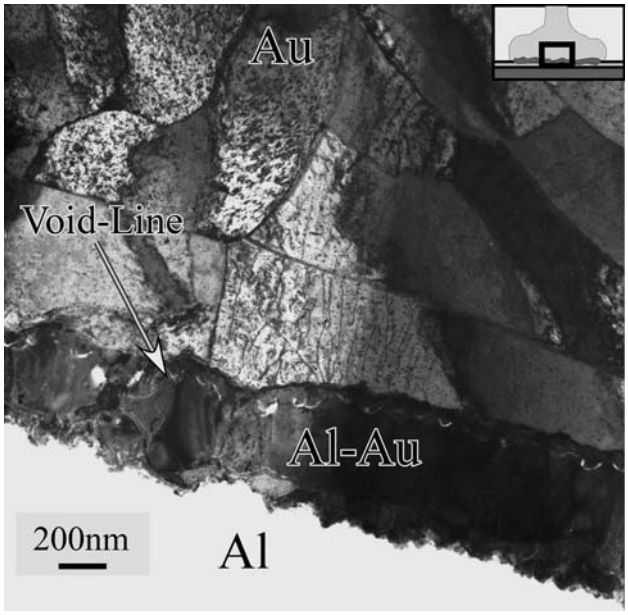

Fig. 6 BF TEM micrograph of the Al–Au region that is formed during the wire bonding process

formed during the wire-bonding process is visible. Our previous study suggests that a liquid forms during bonding, which results in a local volume reduction upon solidification, and the formation of voids in the intermetallic region. Thus the characteristic void-line is not related to a solid-state phase transformation that occurs during annealing [16].

SEM analysis of annealed samples

A simulation of the morphological changes that occur during the lifetime of the device was done by thermal annealing at elevated temperatures for different durations of time. The purpose of this test was to accelerate the metallurgical processes that occur during the lifetime of the device, which can result in bond failure. In this study, the annealing temperature was set to 175 °C, and the annealing time was between 30 min and 100 h.

The morphological changes that occur during annealing are presented in the SEM micrographs in Fig. 7a–d, from the regions indicated in the schematic drawings in the insets of each micrograph. Figure 7a, b present SE SEM micrographs of samples annealed for 30 min and 2 h, showing the Al–Au intermetallic region that contains voids. The change in morphology in the intermetallic region was attributed by Noolu et al. to changes in the composition of the different regions [3]. However, SEM-EDS analysis is not suitable for these systems due to the diameter of the interaction volume that exceeds the length-scale of the intermetallic region [13]. Therefore, in the present study, quantitative EDS analysis was conducted by S/TEM-EDS (see next section). The backscattered electron (BSE) SEM micrograph of the bond annealed for 24 h (Fig. 7c) shows the formation of a large void at the periphery. The bright contrast from the intermetallic region indicates, in BSE mode, a larger average value of the atomic number, which can be correlated with a high Au content in the intermetallic region. Figure 7d presents a SE SEM micrograph of a cross-section of a bond annealed for 100 h at 175 °C, showing the transformation of the peripheral void to a crack between the intermetallic and the Au regions.

According to the SEM analysis of annealed samples, annealing at 175 °C for up to 24 h does not result in growth of the void-line that was formed during the wire-bonding process, but rather in the formation and growth of voids at the periphery of the bond, accompanied by growth of the intermetallic region in the Au and the Al pad. Annealing for 100 h at 175 °C results in the formation of cracks at the periphery region, rather than growth of the void-line.

S/TEM-EDS analysis of annealed samples

Samples annealed for 2 h at 175 °C

Two TEM samples were prepared from samples that were annealed for 2 h at 175 °C and characterized by S/TEM-EDS. The morphology of the Al–Au intermetallic region of sample #1 is presented in the HAADF STEM micrograph in Fig. 8. Figure 10 presents the morphology of regions III and IV in sample #2. The morphology of the intermetallic region is composed of four different regions, indicated as region I–IV. Region I is a thin layer with no distinct morphology. Region II contains large equiaxed grains, while region III contains narrow elongated grains, and region IV contains small equiaxed grains. Regions III and IV are separated by the characteristic void-line.

EDS analysis was conducted on the areas indicated in regions II and III in Fig. 8, and the results are summarized in Table 1. According to the EDS results, there is no change in the composition between regions II and III, and the morphological changes are the result of the initial intermetallic formation during the wire bonding process [16].

Due to the relatively large error in the STEM-EDS analysis, confirmation of the intermetallic structure was done by selected area electron diffraction (SAD) acquired from grains in the different regions. Fig. 9a presents a BF TEM micrograph of regions I and II in

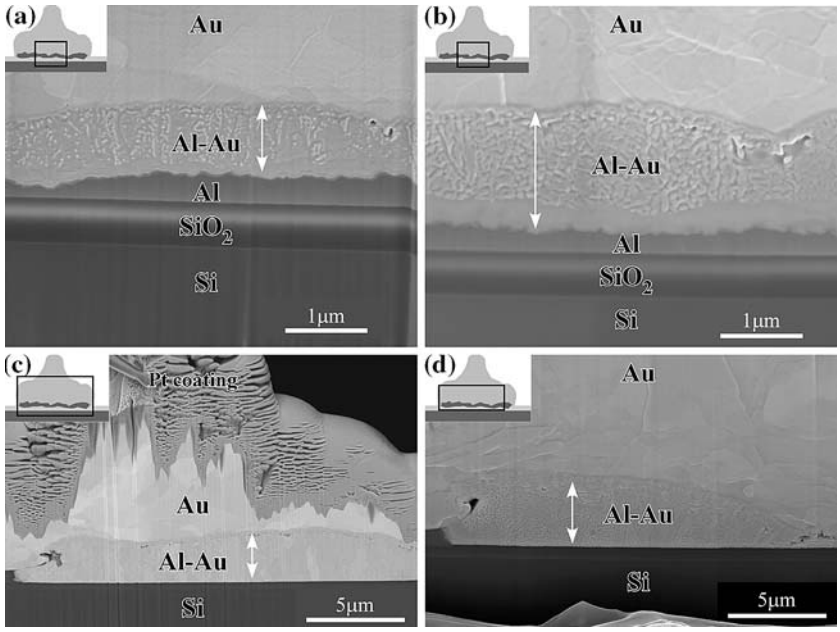

Fig. 7 SEM micrographs of cross-sections of samples annealed for (**a**) 30 min (SE), (**b**) 2 h (SE), (**c**) 24 h (BSE) and (**d**) 100 h (SE)

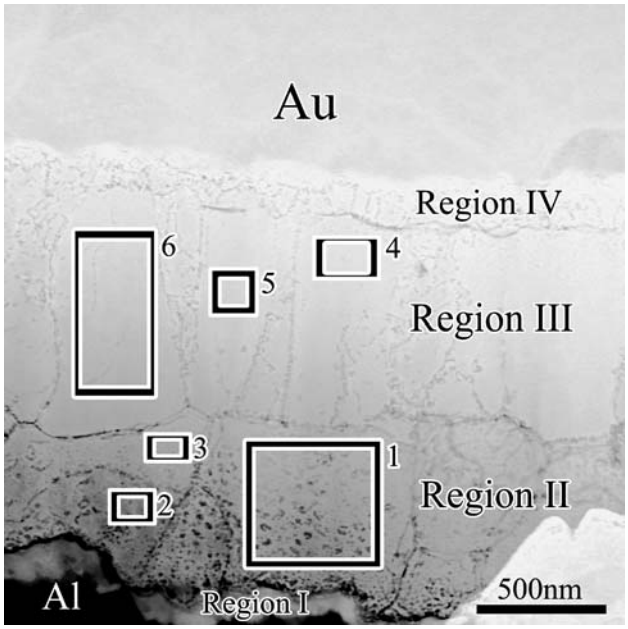

Fig. 8 HAADF STEM micrograph of the Al–Au region is sample #2. EDS analysis was conducted on the indicated areas

sample #1. The SAD acquired from the grain indicated by the dashed line is presented in Fig. 9b. The SAD confirms the Al_3Au_8 structure in a $[\bar{1}\bar{1}20]$ zone-axis. Figure 10a presents a BF TEM micrograph of the intermetallic phases in regions III and IV in sample #2, which was annealed for 2 h at 175 °C. A SAD from the grains, indicated by the dashed line in Fig. 10a, is presented in Fig. 10b. The SAD confirms the existence of Al_3Au_8 and $AlAu_4$. According to the electron diffraction analysis, regions II and III contain the Al_3Au_8 intermetallic and region IV contains the $AlAu_4$ intermetallic phase.

The growth mechanism of the intermetallic region near the Al pad was analyzed by HAADF STEM-EDS, as presented in Fig. 11a. A bright contrast from the Al grain boundaries is visible, which suggests the presence of excess Au at the Al grain boundaries. This was confirmed by the EDS line-scan in Fig. 11b that was conducted from the line indicated in Fig. 11a. According to these results, the intermetallics in the Al region are formed by grain boundary diffusion of Au.

Samples annealed for 72–100 hours at 175 °C

Figure 12a presents a BF TEM micrograph of the bond periphery, from the region close to the substrate. The results of the EDS analysis are summarized in Table 2 and indicate the presence of Au-rich intermetallics. Point 1 and 2 are at the edge of the ball where residual Al exists. EDS analysis from point 1 and 2 indicates nearly equal amounts of Al and Au. Approximately 200 nm from the periphery, SAD from the grain indicated by dashed lines in Fig. 12a confirms the presence of Al_3Au_8 (Fig. 12b). This means that during annealing, Al_3Au_8 is formed by grain boundary diffusion of Au in the Al pad, in the periphery region of the bond where intermetallics were not formed inside the Au.

After annealing for 100 h at 175 °C, cracks started to form inside the bond region. FIB-SEM analysis of annealed bonds showed two stages of failure that occur during annealing, as presented in Fig. 13. Figure 13a

Table 1 EDS results of regions 1–6 in Fig. 8

	1	2	3	4	5	6
Al (K) [at.%]	12 ± 2	13 ± 3	12±3	12 ± 3	11 ± 2	13 ± 3
Au (L) [at.%]	88 ± 13	88 ± 13	88 ± 3	88 ± 3	89 ± 13	88 ± 13

Table 2 EDS results from the regions indicated in Fig. 12

	Point 1	Point 2	Area 1	Area 2
Al (K) [at.%]	55 ± 11	47 ± 9	13 ± 3	13 ± 3
Au (L) [at.%]	52 ± 8	50 ± 8	81 ± 12	80 ± 2
Si (K) [at.%]	3 ± 1	3 ± 1	5 ± 1	5 ± 1

shows a crack initiated at the periphery region of the bond. Figure 13b shows a continuous crack that separates the entire Au ball-bond from the intermetallic region.

Figure 14 presents a HAADF STEM micrograph of the periphery region of a bond containing a crack. The crack propagates between the Al–Au intermetallic region and the Au ball, and not inside the intermetallic

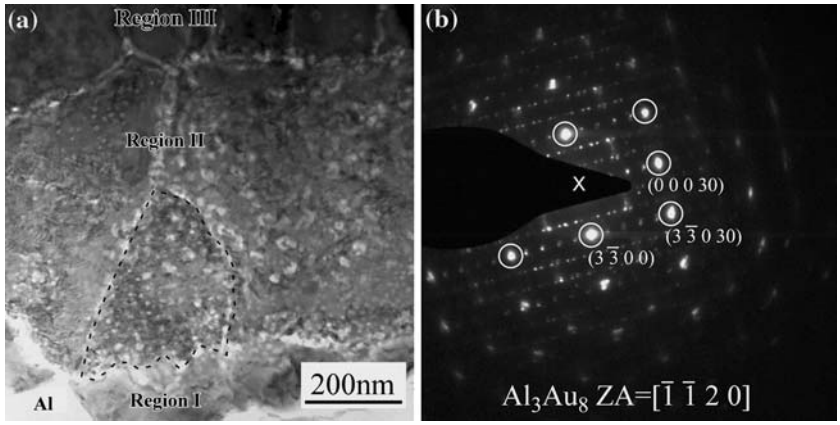

Fig. 9 (**a**) BF TEM micrograph of regions I and II in sample #2. (**b**) SAD from the grain indicated by dashed lines in (**a**) confirms the Al_3Au_8 structure in a [$\bar{1}\bar{1}$20] zone-axis

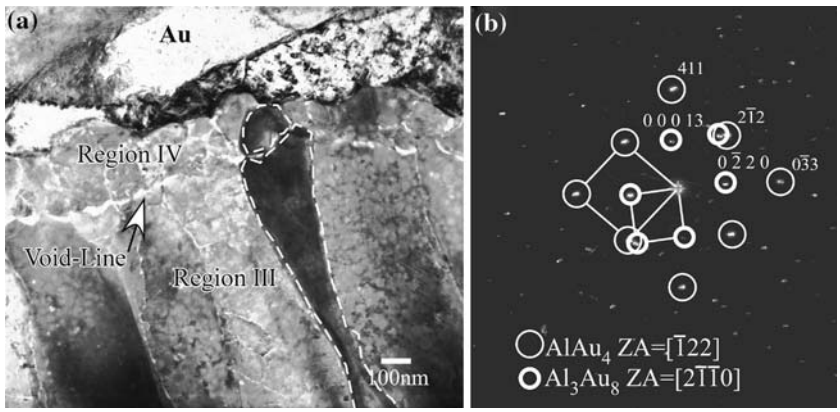

Fig. 10 (**a**) BF TEM micrograph of region III and IV in sample (#1) which was annealed for 2 h. (**b**) SAD from the grains indicated by dashed lines in (a), confirming the existence of the low-temperature stable phase of $AlAu_4$ in a [$\bar{1}$22] zone axis, and Al_3Au_8 in a [2$\bar{1}\bar{1}$0] zone axis

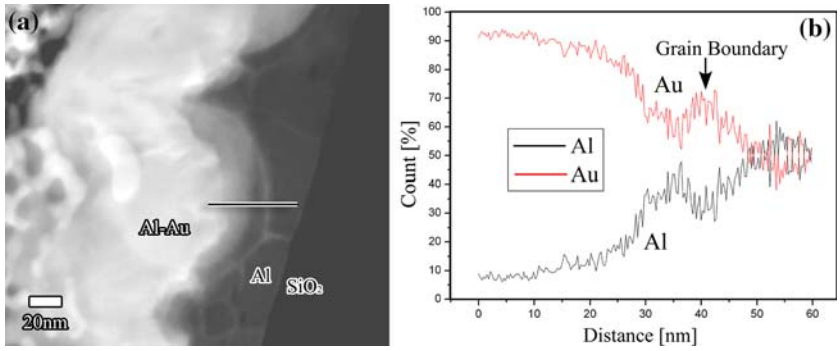

Fig. 11 (**a**) HAADF STEM micrograph of region I and the residual Al pad. (**b**) EDS line-scan conducted on the marked line in (a), indicating an increase in Au concentration at the Al grain boundaries

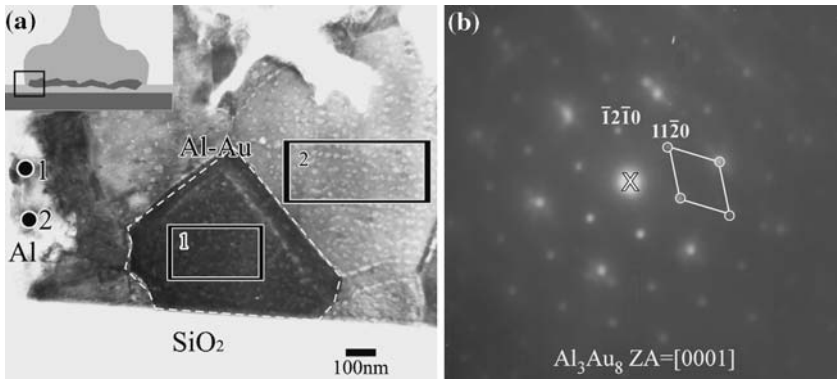

Fig. 12 (**a**) BF TEM micrograph from the periphery region (indicated by the schematic drawing in the inset) of a sample annealed for 72 h. EDS analysis was conducted on the marked regions (see Table 2). (**b**) SAD from the grain indicated by dashed lines in (a) confirms the Al_3Au_8 structure in a [0001] zone axis

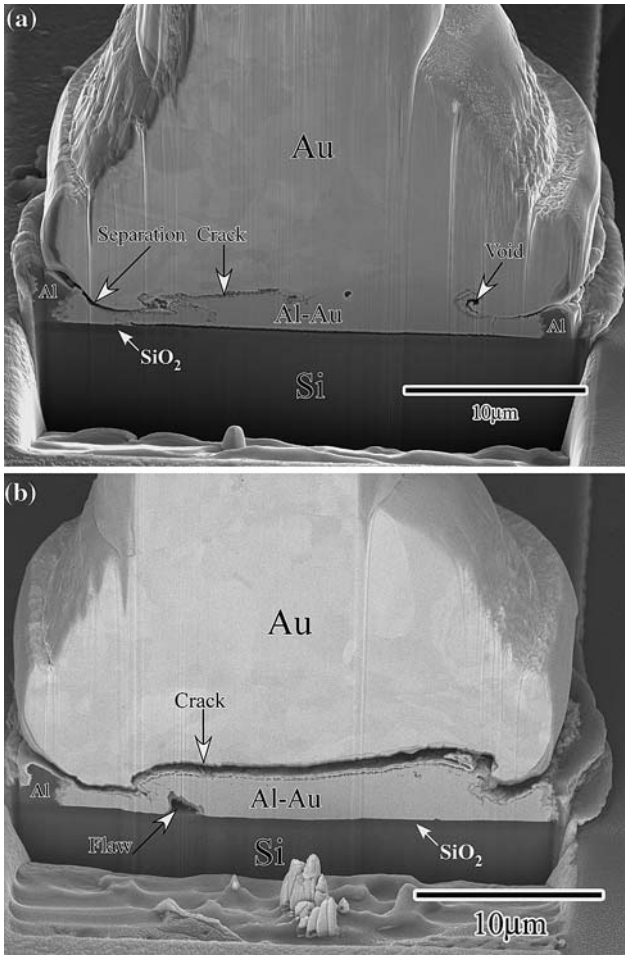

Fig. 13 (**a**) SE SEM micrograph of a cross-section of a sample annealed for 100 h at 175 °C, showing cracks at the bond periphery. (**b**) BSE SEM micrograph of a sample annealed under the same conditions, showing complete separation of the Au ball from the intermetallic region by a crack

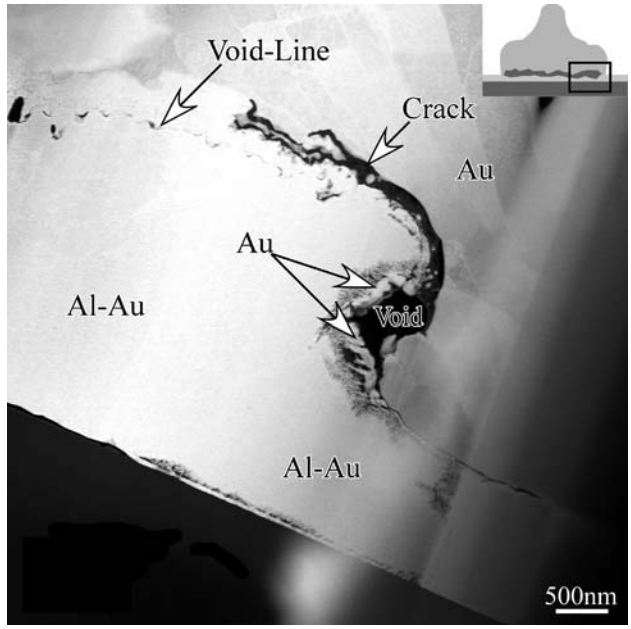

Fig. 14 HAADF STEM micrograph of the periphery region (indicated by the schematic drawing in the inset) showing a void-line inside the intermetallic region, a large periphery void, and a crack

region by growth of the void-line. The characteristic void-line that is formed during the wire-bonding process and is present inside the intermetallic region, does not play an obvious role in formation of the crack. The large void at the bond periphery is directly connected to the crack that is formed between the Au ball-bond and the Al–Au intermetallics. EDS analysis, conducted on the region around the void, showed that the large void at the bond periphery formed inside the Au ball region, and not inside the Al–Au intermetallic region. The morphology of the void is in the form of a crack, which suggests that the void is formed by mechanical stresses rather than a diffusion process.

Figure 15 presents a BF TEM micrograph of the lower crack region from a bond with a crack of the type shown in Fig. 13b, where complete separation occurred between the Au ball and the intermetallic region. A SAD from the grain, marked by the dashed lines in Fig. 15a, confirms the low temperature $AlAu_4$ structure and traces of Al_3Au_8. Figure 16 presents a HA-ADF STEM micrograph of the same region that is

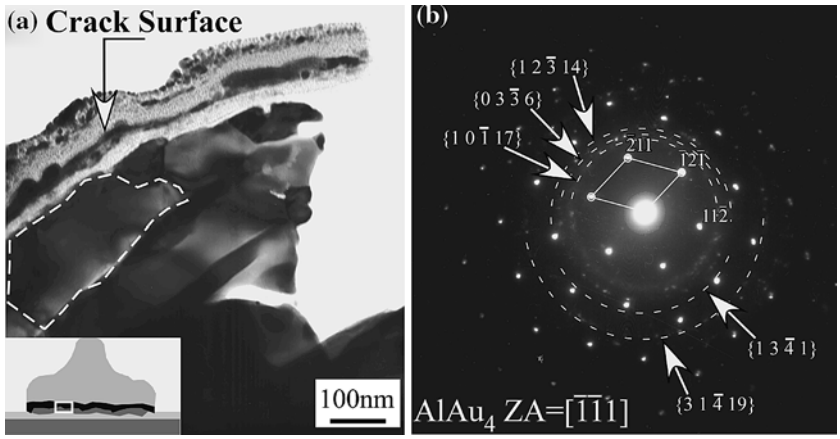

Fig. 15 BF TEM micrograph (**a**) of the lower part of the crack presented in Fig. 13, and a SAD (**b**) from the grain indicated by the dashed line in (a), confirms the presence of $AlAu_4$ and Al_3Au_8

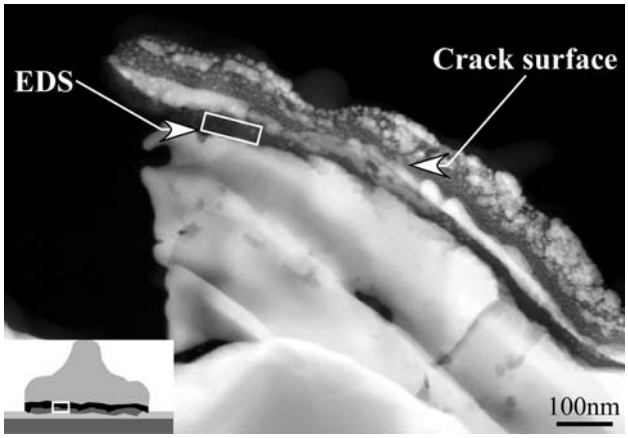

Fig. 16 HAADF STEM micrograph of the lower crack region that is presented in Fig. 15. EDS analysis conducted on the dark regions (indicated by the arrow) indicates the presence of Al and Al_2O_3 (see Table 3)

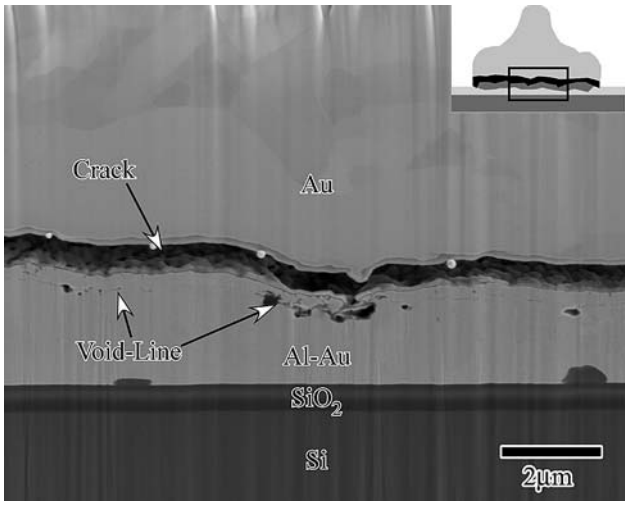

Fig. 17 SE SEM micrograph of the crack region of a bond annealed for 100 h at 175 °C, with the type of failure shown in Fig. 13b. The void line *inside* the intermetallic region, located *below* the crack, is visible

Table 3 EDS results from the dark region on the surface of the crack, indicated by the arrow in Fig. 16

Al (K) [at.%]	53 ± 8
Au (L) [at.%]	0.8 ± 0.2
O (K) [at.%]	44 ± 7

presented in Fig. 15. A dark contrast is present in the crack region, which, in HAADF STEM mode, can be associated with the presence of light atomic weight elements. EDS analysis was conducted on the dark regions in the crack (see Table 3), which indicates that a diffusion process of Al out of the intermetallic region results in the formation of Al_2O_3. The presence of a brittle region between the intermetallics and the Au ball results in crack formation by brittle fracture.

Figure 17 is a SE SEM micrograph of the crack region presented in Fig. 13b at a higher magnification. The characteristic void-line is present inside the intermetallic region *under* the crack, which means that the formation of the void-line during the wire bonding process does not result in the formation of a crack.

Discussion

During the wire bonding process, the bond is created by the formation of intermetallics at the Al–Au interface, due to the application of ultrasonic and thermal energy [1]. An examination of the intermetallic region that is formed during the wire-bonding process of Au to Al (Fig. 1) showed that plastic deformation of the initial FAB results in the formation of a periphery region that does not contain intermetallics. This can result in the formation of a bonding gap [11]. This means that a direct connection is not achieved in the periphery region of the bond. Therefore, growth of the intermetallic region during annealing, which results in

volume changes [2, 3], can cause the formation of stresses between the residual Au at the periphery region and the intermetallics in the bond region.

Analysis of the morphology of the Au ball-bond and the intermetallic region that is formed during the wire-bonding process, *prior* to the annealing treatments, showed that the characteristic void-line that is found inside the intermetallic region is formed during the wire bonding process, which is a relatively fast process. Therefore, void formation cannot occur as a result of diffusion mechanisms such as the Kirkendall phenomenon. Our previous work suggested that a local solid–liquid transformation occurs during the bond formation, and shrinkage of the intermetallic region upon solidification results in the formation of voids [16]. The present work deals with the question of whether the formation of the void-line results in failure by crack formation during annealing.

Microstructural analysis of samples annealed for 2 h at 175 °C found Au rich intermetallics. SAD from grains in the different intermetallic regions confirmed the presence of Al_3Au_8 and $AlAu_4$. No indication to the formation of other thermodynamically stable intermetallics was found by this analysis. Our previous work [16] showed that the microstructure of the intermetallic region strongly depends on the Al pad content, where the additions of Si and Cu to the Al pad influence the microstructure of the intermetallics that are formed during the bonding process.

The growth mechanism in the Al pad region was found to occur by grain boundary diffusion of Au through the Al, which is a relatively fast process in comparison to bulk-diffusion. SEM analysis of the interface regions of bonds annealed for 24 h (or more) at 175 °C showed that during annealing, the Al pad under the bond transforms into Au-rich intermetallics. No transformation of Au to Al–Au intermetallics occurred in the periphery region of the bond where the intermetallic did not form during the wire bonding process. This can be attributed to the formation of the gap during the wire bonding process [11].

During annealing, a characteristic void is formed in the periphery region of the bond between the Au and the intermetallics (Figs. 7, 13a, and 14). This can be attributed to volume changes that occur during the formation of Al–Au intermetallics both in the Au region and in the Al pad under the bond. In order to understand the change in volume during intermetallic formation, the amount of volume that the atoms occupy in the lattice was calculated by the atomic packing factor (A.P.F.) of Al, Au, Al_3Au_8 and $AlAu_4$, as presented in Table 4. Al and Au are face centered cubic (FCC) metals, having the highest packing density, and their transformation to intermetallics with a lower A.P.F results in an increase in volume of the system. It is likely that this increase in volume results in local stresses, which in turn results in the formation of a crack and separation between the intermetallic region and the Au ball-bond, as presented in Fig. 14.

Table 4 The A.P.F of Al, Au and the intermetallics that are formed during annealing

	A.P.F.
Al	0.74
Au	0.74
Al_3Au_8	0.25
$AlAu_4$	0.72

Complete separation of the Au ball from the intermetallic region was identified after annealing for 100 h at 175 °C (Fig. 13b). S/TEM-EDS analysis of the crack region showed the presence of Al and Al_2O_3 at the surface of the crack, above the $AlAu_4$ grains. Surface analysis of the aluminide intermetallic showed that diffusion of Al to the surface occurs during annealing, resulting in the formation of Al_2O_3 at free surfaces and grain boundaries of the aluminide intermetallics. The formation of Al_2O_3 is suspected to result in intergranular fracture [18, 19]. In the present study, the diffusion of Al results in an Al layer between the intermetallic region and the Au ball bond. The gap that was formed during the wire bonding process can result in the penetration of oxygen to the Al region and its oxidation.

During extended annealing, the cracks are formed and propagate between the Au and the intermetallic region, and *not* by growth of the characteristic void-line that was formed prior to annealing during the bonding process. Failure by cracking can occur by two mechanisms. The first is volume changes during intermetallic formation that results in plastic deformation of the Au ball-bond and the formation of a crack initiated at the periphery region of the bond (Fig. 13a). The second mechanism is oxidation of the intermetallic surface after diffusion of Al from the intermetallic to the Au-intermetallic interface. The formation of a brittle region at the Au-intermetallic interface can result in brittle facture, as presented in Fig. 13b.

Summary and conclusions

During exposure to elevated temperatures, the intermetallic region at the interface of the bonds grows by diffusion. The transformation of Al to an intermetallic

occurs by diffusion of Au through the Al grain boundaries, which results in the formation of an Au-rich intermetallic region both under the Au ball and in the periphery region of the ball. The transformation to Al–Au intermetallics results in an increase of volume and deformation of the Au ball. This can result in stress-induced cracks at the periphery region of the ball and degradation of the bond strength. In addition, the formation of cracks results in the oxidation of the intermetallic region adjacent to the Au ball, which in turn results in the formation of a continuous crack. The void-line that is found in the intermetallic region does not take part in bond failure. Therefore, two mechanisms are responsible for the degradation of the bond: an increase of volume by intermetallic formation, which results in stress induced cracks; and oxidation of the interface between the Au and the intermetallics. In order to overcome this failure, an increase of the Au durability to plastic deformation should be achieved.

Acknowledgements The authors thank the Russell Berrie Nanotechnology Institute at the Technion for use of the FIB, and I. Popov for assistance with use of the TEM.

Appendix

	Structure Type	Pearson Symbol	Space Group	Lattice parameters (nm)
Al_3Au_8 [20]	Al_3Au_8	hR44	$R\bar{3}c$	$a = 0.7724$ $c = 4.2083$
$AlAu_4$ [19]	$AlAu_4$	cP20	$P2_13$	$a = 0.6902$

References

1. Harman G (1997) Wire-bonding in microelectronics materials process reliability and yield. McGraw-Hill Publishers, NY
2. Zhang X, Yan TT (2006) Thin Solid Films 504[1–2]:355
3. Noolu NJ, Murdeshwar NM, Ely KJ, Lippold JC, Baeslack WA (2004) J Mater Res 19(5):1374
4. Breach CD, Tok CW, Wulff F, Calpito D (2004) J Mater Sci 39(19):6125
5. Maiocco L, Smyers D, Kadiyala S, Baker I (1990) Mater Charact 24(4):293
6. Clatterbaugh GV, Weiner JA, Charles HK (1984) IEEE Trans Compon Hybrids Manufacture Technol 7(4):349
7. Majni G, Nobili C, Ottaviani G, Costato M, Galli E (1981) J Appl Phys 52(6):4047
8. Markwitz A, Matz W (1970) Surf Interface Anal 26(9):650
9. Philofsky E (1970) Solid-State Electron 13(10):1391
10. Xu C, Sritharan T, Mhaisalkar SG (2007) Scripta Mater 56(6):549
11. Chang HS, Hsieh KC, Martens T, Yang A (2004) IEEE Trans Compon Pack Technol 27(1):155
12. Ji H, Li M, Wang C, Bang HS, Bang HS (2007) Mater Sci Eng A 447(1–2):111
13. Williams DB, Carter BC (1996) Transmission electron microscopy. Plenum, New York
14. Karpel A, Kaplan WD, Atzmon Z, Gur G (2005) In: Havas D, Levine L (eds) Proceedings of the 2005 international symposium on microelectronics, IMAPS. p 325
15. Reyntjens S, Puers R (2001) J Micromech Microeng 11(4):287
16. Karpel A, Gur G, Atzmon Z, Kaplan WD (2007) J Mater Sci, in press. doi 10.1007/s10853-007-1592-z
17. Bowden P, Brandon DG (1963) J Nuclear Mater 9(3):348
18. Piao H, McIntyre NS (2001) Surf Interface Anal 31(9):874
19. Xu C, Breach CD, Sritharan T, Wulff F, Mhaisalkar SG (2004) Thin Solid Films 462–463:357
20. Villars P (1991) Pearson's handbook of crystallographic data for intermetallic phases, 2nd ed. vol 1. ASM International, Materials Park, Ohio, p 652